Communication

Helical Rosette Nanotubes with Tunable Stability and Hierarchy

Jesus G. Moralez, Jose Raez, Takeshi Yamazaki, R. Kishan Motkuri, Andriy Kovalenko, and Hicham Fenniri

J. Am. Chem. Soc., **2005**, 127 (23), 8307-8309• DOI: 10.1021/ja051496t • Publication Date (Web): 21 May 2005

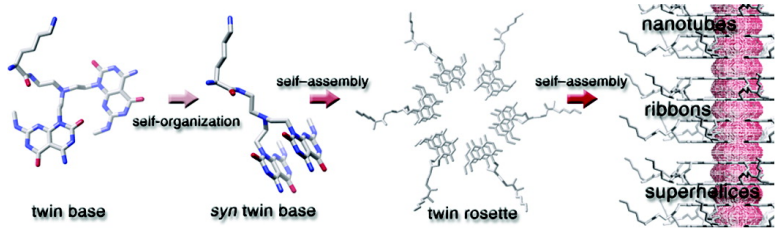

More About This Article

Additional resources and features associated with this article are available within the HTML version:

- Supporting Information
- Links to the 9 articles that cite this article, as of the time of this article download
- Access to high resolution figures
- Links to articles and content related to this article
- Copyright permission to reproduce figures and/or text from this article

View the Full Text HTML

J|A|C|S
COMMUNICATIONS

Published on Web 05/21/2005

Helical Rosette Nanotubes with Tunable Stability and Hierarchy

Jesus G. Moralez,[†,‡] Jose Raez,[†,‡] Takeshi Yamazaki,[†,¶] R. Kishan Motkuri,[†,‡] Andriy Kovalenko,[†,¶] and Hicham Fenniri*[,†,‡]

National Institute for Nanotechnology (NINT-NRC), Department of Chemistry, and Department of Mechanical Engineering, University of Alberta, ECERF 9107-116 Street, Edmonton, Alberta T6G 2V4, Canada

Received March 9, 2005; E-mail: hicham.fenniri@nrc-cnrc.gc.ca

Supramolecular synthesis[1] emerged over the past decade as a new formalism to devise complex architectures held through noncovalent forces. Much of the research endeavor has been devoted to the use of H-bonds as the alphabet for chemical information encoding, and the structures expressed have spanned the range of dimensions and shapes, from discrete[1,2] to infinite[1f,3,4] networks.

The G∧C motif (Figure 1A) was recently shown to undergo a hierarchical self-assembly process fueled by hydrophobic effects in water to form a six-membered supermacrocycle maintained by 18 H-bonds (rosette, Figure 1B). The resulting and substantially more hydrophobic aggregate self-organizes into a linear stack defining an open central channel 1.1 nm across and several micrometers long (Figure 1D).[4] In principle, upon self-assembly, any functional group covalently attached to the G∧C motif could be expressed on the surface of the nanotubes, thereby offering a general "built-in" strategy for tailoring the physical and chemical properties of the helical rosette nanotubes (HRNs). However, the stability of the resulting aggregate is anticipated to depend on functional group density (sterics) and net charge (electrostatics) on the HRN surface. Here, we describe a strategy that allowed us to probe the extent to which these factors affect the supramolecular outcome and use that knowledge to tune the stability and hierarchical organization of these materials. Thus, compounds **1**−**3** were synthesized with three elements in mind: (a) **1** has one net positive charge, whereas **2** and **3** have three; (b) **1** and **2** feature a single G∧C base, whereas **3** has two (twin bases); and (c) **3** has three protonation sites ($pK_a^1 \sim 10.03$, $pK_a^2 \sim 8.28$, $pK_a^3 \sim 7.68$) in the pH range of 4 to 11.[5]

Compound **1** was previously shown to undergo self-assembly into HRN by NMR spectroscopy, mass spectrometry, circular dichroism (CD) spectroscopy, variable temperature UV−vis melting studies, dynamic light scattering (DLS), tapping mode atomic force microscopy (TM-AFM), and transmission electron microscopy (TEM).[4a] In agreement with the calculated average diameter of 3.2 nm,[6] TEM (Figure 2A) and TM-AFM images (Figure 2B) of HRN **1** featured a diameter of 3.4 ± 0.3 and 3.2 nm, respectively. Compound **2**, which differs from **1** by its higher net charge (3+ versus 1+), did not show any evidence of aggregation by AFM and TEM (data not shown). While the DLS spectrum of **1** (1 mg/mL) showed the formation of aggregates with an apparent hydrodynamic diameter, D_h, of 36 nm (∼95% in the range of 25−50 nm), the light scattering signal of **2** was undetectable. At 5 and 10 mg/mL, the DLS signal for **2** improved, allowing us to estimate D_h, which for both cases was ∼1 nm.[6] Although this value is unreliable since it is at the lower detection limit of DLS, it suggests that **2** did not aggregate even at 10 times the concentration of **1**. Furthermore, comparison of the UV−vis extinction coefficients at

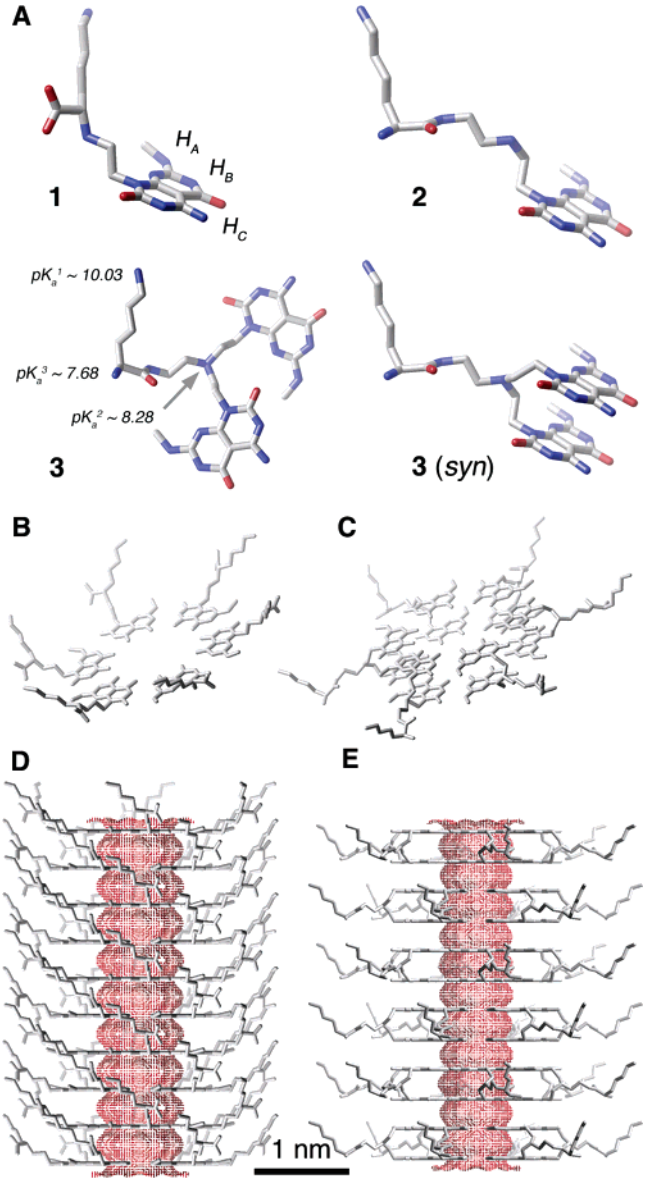

Figure 1. G∧C derivatives **1**−**3** investigated (A). Single (B) and twin (C) rosettes obtained from the self-assembly of **1** and **3**, respectively. Rosette nanotubes obtained from **1** (D) and **3** (E). The inner channel is highlighted in red.

λ_{max} for **1**−**3** showed a hyperchromic effect in the case of **2**, suggesting that the latter does not form stacked aggregates.[6]

To further validate the electrostatics/sterics hypothesis, twin base compound **3** (Figure 1A) was prepared.[6] Due to their hydrophobic character and the spacer length separating them (5 atoms), the G∧C bases in **3** were anticipated to self-organize into a syn (CH_3NH_A on the same side) or anti stack (CH_3NH_A on opposite sides).

† National Institute for Nanotechnology.
‡ Department of Chemistry.
¶ Department of Mechanical Engineering.

10.1021/ja051496t CCC: $30.25

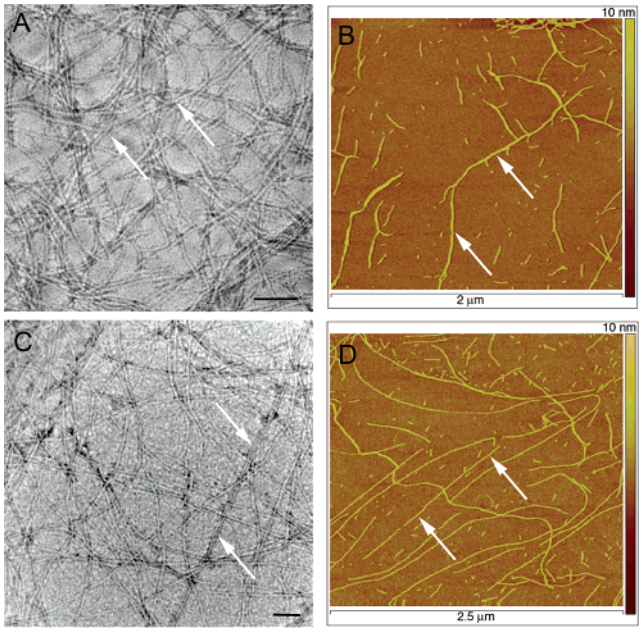

Figure 2. Negatively stained TEM micrographs (scale bar = 50 nm) and TM-AFM images of HRN obtained from **1** (A and B) and **3** (C and D), respectively (pH 5.5, unbuffered). TEM samples were prepared by carbon grid floating, and AFM samples were prepared by spin coating on Si/SiH_x.[6] Arrows point at individual nanotubes.

Furthermore, because the G∧C base H-bond arrays are asymmetric, the resulting rosettes should be composed of all-syn or all-anti conformers (self-selection) in order to maximize the number of H-bonds. TOCSY, COSY, and NOESY NMR studies showed only one set of protons for the exocyclic methylamino groups,[6] suggesting that only one conformer is present. This result is also in agreement with molecular modeling studies[6] that favored the rosette formation of the syn over the anti conformers by 8.4 kcal/mol. The self-assembly of the syn conformer could yield a single rosette with up to six dangling bases or a twin rosette where the G∧C bases are all in register (blunt end). The latter is anticipated to be thermodynamically more favorable and is in agreement with the NMR, TEM, and AFM data. On the basis of these premises, **3** was designed so that upon self-assembly (a) the functional group density and net charge are reduced by a factor of 2 compared to **2**, (b) the thermal stability of the nanotubes is enhanced as a result of preorganization, increased amphiphilic character, and greater number of H-bonds per module (12 instead of 6), (c) the corresponding double rosettes are preorganized and maintained by 36 H-bonds instead of 18 (Figure 1C), and (d) the resulting HRN (Figure 1E) is sterically less congested and experiences reduced electrostatic repulsion on its surface.[6]

Two-dimensional water-gate NOESY (800 MHz, 90% H_2O/D_2O) of **3** displayed nuclear Overhauser effects (NOEs) not only between H^A and H^B but also between H^B and H^C.[6] Since H^B and H^C are too far apart to display any *intra*modular NOEs, the observation of an NOE between them confirms the existence of *inter*modular H-bonds, as highlighted in Figure S3.[6] This result is also diagnostic of the formation of the rosette structure since no other NOEs or imino proton signals resulting from nonassembled **3** or nonspecific aggregates thereof were observed. TEM (Figure 2C) and TM-AFM images (Figure 2D) of HRN **3** featured a diameter of 4.0 ± 0.3 and 3.3 nm, respectively, in agreement with the calculated average diameter of 3.8 nm.[6] The DLS spectrum of an aqueous solution of **3** (1 mg/mL) showed the presence of aggregates with an apparent hydrodynamic diameter, D_h, of 11 nm (95% in the range of 8−18 nm).[6]

The CD spectrum of an aqueous solution of **1** displays a typical couplet centered at 286 nm,[6] characteristic of stacked bases in a helical environment, that decreases with increasing temperature and vanishes at 85 °C.[6] While an aqueous solution of **2** was CD-silent in the range of 200−800 nm, **3** revealed a strong CD couplet centered around 247 nm, the intensity of which persisted even at 95 °C (50% of the intensity at 25 °C).[6] This enhanced thermal stability along with NMR, AFM, TEM, and DLS studies corroborate our design criteria.

In support of these results, molecular models of HRN **1** and **3** were generated using Macromodel 8.5/Maestro 6.0, and the thermodynamic characteristics of HRN hydration were derived using the 3D-RISM/KH theory.[6,7] The association energy of six molecules of **1** into a rosette in water was found to be 101 kcal/mol (5.6 kcal/mol per hydrogen bond). The association energy of six hydrated twin base modules of **3** into a twin rosette of the syn conformers was calculated to be 770 kcal/mol (21.4 kcal/mol per hydrogen bond). The free energy of stacking of two rosettes in aqueous solution was calculated to be 168 kcal/mol for HRN **1** and 1890 kcal/mol for HRN **3**. The free energy of adding a new rosette to a nanotube increases almost linearly by 206 kcal/mol for each new single rosette in HRN **1** and by 1890 kcal/mol for each new twin rosette in HRN **3**. This linear increase is indicative of an effective electrostatic field that builds up with the nanotube length, which suggests the formation of a macrodipole. These modeling studies predict that the association free energy of HRN **3** of any length is about twice that of HRN **1** of the same length, confirming the success of our strategy in the synthesis of HRNs with tunable stability.

To investigate the effect of net electrostatic charge on the supramolecular organization within the same system, the self-assembly of **3** (1 mg/mL) was monitored at pH 4, 7, and 11 in water by TEM, scanning electron microscopy (SEM),[6] CD spectroscopy, and DLS. At pH 4, the self-assembly of **3** resulted in the formation of HRNs with an outer diameter of 4.0 ± 0.3 nm, in agreement with the calculated diameter of 3.8 nm (Figure 3A). Their length, however, was significantly shorter compared to that measured at pH 5.5 (Figure 2C) and showed a bimodal distribution, in agreement with the DLS studies.[6] The average nanotube length was 160 ± 111 nm, corresponding to a polydispersity index of 1.44. At pH 7, while their length exceeded 5 μm, most of the HRNs aggregated laterally in the form of ribbons with up to 39 nm in width (Figure 3B,C). At pH 11, the HRNs evolved into uniform right-handed superhelices composed of ∼32 HRNs, with 141 ± 30 nm in width, up to 7.5 μm in length, a helical pitch of 901 ± 55 nm, and an inclination angle of 51 ± 12° (Figure 3D−I).

This pH study allowed us to capture three aggregation states leading to the hierarchical self-assembly of rosette nanotube superhelices, which were correlated with the protonation states of the L-lysine side chain of module **3** (Figure 1A). When the pH was adjusted to 4, all three basic amino groups of **3** are protonated, thus maximizing intermolecular repulsion and resulting in the formation of relatively short well-dispersed nanotubes (compare Figures 2C and 3A). At pH 7, the α-amino group is partially protonated ($pK_a^3 \sim 7.68$), thus reducing the net charge of **3** to +2 and promoting end-to-end fusion and lateral aggregation into HRN ribbons with relatively uniform width. At pH 11, all basic nitrogens should be unprotonated except for the ϵ-amino group that should be partially protonated ($pK_a^1 \sim 10.03$), thus further reducing charge repulsion and leading to the aggregation of the nanotubes into superhelices. To rule out the possibility of helical twisting due to interaction with the substrate (carbon-coated copper grid), CD experiments were carried out in solution. As expected, the CD spectra at pH 4, 7, and 11 resulted in very different profiles, suggesting

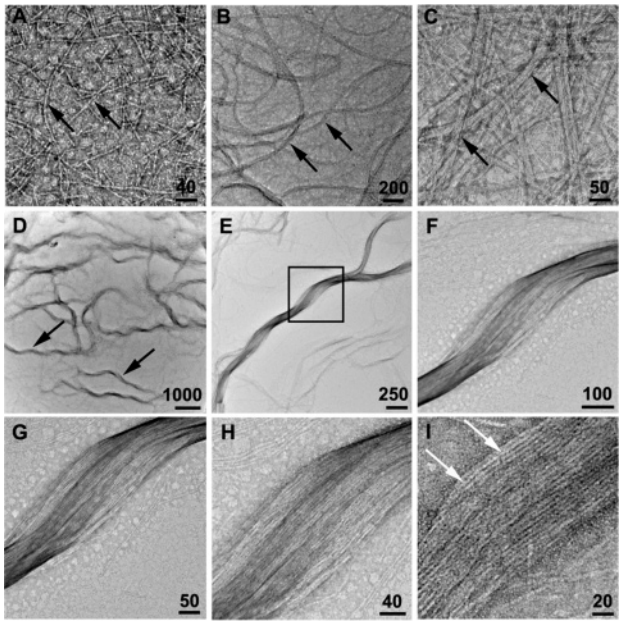

Figure 3. TEM micrographs of negatively stained assemblies obtained from **3**. At pH 4, short well-dispersed helical rosette nanotubes (HRNs) are formed (A). At pH 7, the HRNs aggregate into ribbons (B and C). Black arrows point at individual HRNs in A and at HRN ribbons in B and C. TEM micrographs of superhelices obtained from **3** at pH 11 (D−I). Low-magnification (D−F) and high-magnification (G−I) TEM images of negatively stained HRN superhelices showing their hierarchical organization. The open black box in B highlights the region that was magnified in F−I. Black arrows in D point at superhelices, and white arrows in I point at individual HRNs (∼32 HRNs per superhelix). Scale bars are in nanometers.

the formation of different superstructures in solution, as well.[6] On the basis of these results, we propose that the ribbons observed at pH 7 act as precursors to the superhelices observed at pH 11.

Dislocations of molecular disks that assemble into a supramolecular nanofiber have been proposed to be the source of superhelical coiling.[8a] However, the origin of the superhelical twist observed here is unique and subtle as it is clear that the HRNs do not twist around one another when they aggregate, but they rather pack in a parallel (or antiparallel) fashion along the main axis of the ribbon at both pH 7 and 11 (Figure 3C,G−I). Therefore, the superhelical twist of the ribbons at pH 11 must arise from (a) the collective chirality of the individual nanotubes when the width of the ribbons reaches a critical value (∼140 nm), and (b) a reduced charge repulsion that could possibly lead to the formation of intertube interactions. In the latter case, a simple model, in which the L-lysine side chains of two antiparallel HRNs were interdigitated, was generated and energy-minimized.[6] The model did indeed evolve rapidly toward a right-handed helical ribbon. In the case of amphiphilic bilayer systems, helical ribbons are considered to be intermediate states since they eventually coil to form tubules.[8b−d] The coiling of such helical ribbons is mainly caused by the lateral surface tension along the edges and the chirality of the molecules. In the present case, such lateral surface tension is nonexistent since the edges of the ribbons are hydrophilic, which may explain why the HRN superhelices do not evolve into tubules.

Hierarchical self-assembly is a process by which natural systems converge small components into complex functional architectures. Achieving the design of supramolecular nanostructures with a hierarchical order that parallels the complexity of natural systems requires in-depth understanding of the forces that orchestrate their organization, and the characterization of intermediate states leading to the final superstructure. Here, we have shown how a single small synthetic organic molecule undergoes a series of at least five organizational and self-assembly steps to form complex, yet, well-defined supramolecular architectures. In particular, this study allowed us not only to establish the role of electrostatic and steric factors on the self-assembly process in water but also to use this knowledge to tune the stability and supramolecular architecture of the resulting assemblies. From these studies, we may also postulate that a G∧C module bearing chiral, neutral peptides or chiral hydrocarbon pendants may undergo self-assembly into HRN tubules via the formation of interdigitated β-sheets or bilayers, respectively. Work to test these hypotheses and to explore the extent to which our design principles will hold are currently being tested in the supramolecular synthesis of dendritic nanotubes.

Acknowledgment. We thank NSERC, NRC, and the University of Alberta for supporting this program. We thank the Canadian National High Field NMR Centre (NANUC) for their assistance and use of the facilities. J.G.M. thanks NIH (GM55146-08) for a graduate fellowship.

Supporting Information Available: Synthetic scheme for the preparation of **2** and **3**, NMR data, UV−vis spectra, CD and VT CD studies, DLS spectra, TEM and SEM images, sample preparation and imaging procedures, and computational methods. This material is available free of charge via the Internet at http://pubs.acs.org.

References

(1) (a) Whitesides, G. M.; Simanek, E. E.; Mathias, J. P.; Seto, C. T.; Chin, D. N.; Mammen, M.; Gordon, D. M. *Acc. Chem. Res.* **1995**, *28*, 37−44. (b) Prins, L. J.; Reinhoudt, D. N.; Timmerman, P. *Angew. Chem., Int. Ed.* **2001**, *40*, 2382−2426. (c) Reinhoudt, D. N.; Crego-Calama, M. *Science* **2002**, *295*, 2403−2407. (d) Stoddard, J. F.; Tseng, H.-R. *Proc. Natl. Acad. Sci. U.S.A.* **2002**, *99*, 4797−4800. (e) Lehn, J.-M. *NATO ASI Series E: Appl. Sci.* **1996**, *320*, 511−524. (f) Mascal, M. *Contemporary Org. Synth.* **1994**, *1*, 31−46.

(2) (a) MacGillivray, L. R.; Atwood, J. L. *Angew. Chem., Int. Ed.* **1999**, *38*, 1018−1033. (b) Müller, A.; Reuter, H.; Dillinger, S. *Angew. Chem., Int. Ed.* **1995**, *34*, 2328−2361. (c) Hof, F.; Craig, S. L.; Nuckolls, C.; Rebek, J., Jr. *Angew. Chem., Int. Ed.* **2002**, *41*, 1488−1508. (d) Hill, D. J.; Mio, M. J.; Prince, R. B.; Hughes, T. S.; Moore, J. S. *Chem. Rev.* **2001**, *101*, 3893−4011. (e) Lawrence, D. S.; Jiang, T.; Levett, M. *Chem. Rev.* **1995**, *95*, 2229−2260. (f) Zimmerman, S. C.; Lawless, L. J. *Top. Curr. Chem.* **2001**, *217*, 95−120. (g) Leininger, S.; Olenyuk, B.; Stang, P. J. *Chem. Rev.* **2000**, *100*, 853−908. (h) Davis, J. T. *Angew. Chem., Int. Ed.* **2004**, *43*, 668−698.

(3) (a) Philp, D.; Stoddart, J. F. *Angew. Chem., Int. Ed. Engl.* **1996**, *35*, 1155−1196. (b) Melendéz, R. E.; Hamilton, A. D. *Top. Curr. Chem.* **1998**, *198*, 97−129. (c) Etter, M. C. *Acc. Chem. Res.* **1990**, *23*, 120−126. (d) Desiraju, G. R. *Angew. Chem., Int. Ed. Engl.* **1995**, *34*, 2311−2327. (e) Menger, F. M. *Proc. Natl. Acad. Sci. U.S.A.* **2002**, *99*, 4818−4822. (f) Kato, T. *Struct. Bonding* **2000**, *96*, 95−146. (g) Bong, D. T.; Clark, T. D.; Granja, J. R.; Ghadiri, M. R. *Angew. Chem., Int. Ed.* **2001**, *40*, 988−1011. (h) Hartgerink, J. D.; Zubarev, E. R.; Stupp, S. I. *Curr. Opin. Solid State Mater. Sci.* **2001**, *5*, 355−361. (i) MacDonald, J. C.; Whitesides, G. M. *Chem. Rev.* **1994**, *94*, 2383−2420. (j) Brunsveld, L.; Folmer, B. J. B.; Meijer, E. W.; Sijbesma, R. P. *Chem. Rev.* **2001**, *101*, 4071−4097. (k) Cornelissen, J. J. L. M.; Rowan, A. E.; Nolte, R. J. M.; Sommerdijk, N. A. J. M. *Chem. Rev.* **2001**, *101*, 4039−4070.

(4) (a) Fenniri, H.; Mathivanan, P.; Vidale, K. L.; Sherman, D. M.; Hallenga, K.; Wood, K. V.; Stowell, J. G. *J. Am. Chem. Soc.* **2001**, *123*, 3854−3855. (b) Fenniri, H.; Deng, B.-L.; Ribbe, A. E. *J. Am. Chem. Soc.* **2002**, *124*, 11064−11072. (c) Fenniri, H.; Deng, B.-L.; Ribbe, A. E.; Hallenga, K.; Jacob, J.; Thiyagarajan, P. *Proc. Natl. Acad. Sci. U.S.A.* **2002**, *99*, 6487−6492.

(5) The pK_a values of **3** were calculated using ChemAxon Ltd., physical properties prediction software.

(6) See Supporting Information.

(7) (a) Kovalenko, A. Three-Dimensional RISM Theory for Molecular Liquids and Solid−Liquid Interfaces. In *Molecular Theory of Solvation*; Hirata, F., Ed.; Understanding Chemical Reactivity Series, Vol. 24; Mezey, P. G., Ed.; Kluwer Academic Publishers: Dordrecht, The Netherlands, 2003; pp 169−276. (b) Kovalenko, A.; Hirata, F. *J. Chem. Phys.* **2000**, *112*, 10391−10402 and 10403−10417.

(8) (a) Hill, J. P.; Jin, W.; Kosake, A.; Fukushima, T.; Ichihara, H.; Shimomura, T.; Ito, K.; Hashizume, T.; Ishii, N.; Aida, T. *Science* **2004**, *284*, 1481−1483. (b) Fuhrhop, J.-H.; Helfrich, W. *Chem. Rev.* **1993**, *93*, 1565−1582. (c) Jung, J. H.; John, G.; Yoshida, K.; Shimizu, T. *J. Am. Chem. Soc.* **2002**, *124*, 10674−10675. (d) Oda, R.; Huc, I.; Schmutz, M.; Candau, S. J.; MacKintosh, F. C. *Nature* **1999**, *399*, 566−569.

JA051496T